RELATIONSHIP BETWEEN LOCAL AND EFFECTIVE AERODYNAMIC PITCH-DAMPING DERIVATIVES AS MEASURED BY A FORCED-OSCILLATION BALANCE FOR PRELIMINARY VIKING CONFIGURATIONS

J. P. Billingsley and W. S. Norman

ARO, Inc.

May 1972

AD 741769

D D C

MAY 16 1972

C

Approved for public release; distribution unlimited.

VON KÁRMÁN GAS DYNAMICS FACILITY
ARNOLD ENGINEERING DEVELOPMENT CENTER
AIR FORCE SYSTEMS COMMAND
ARNOLD AIR FORCE STATION, TENNESSEE

53

R

NOTICES

ACCESSION for
OFSTI   WHITE SECTION
DDC   BUFF SECTION
UNANNOUNCED
JUSTIFICATION

BY.
DISTRIBUTION/AVAILABILITY CODES
DIST.   AVAIL. and or SPECIAL

RELATIONSHIP BETWEEN LOCAL AND EFFECTIVE AERODYNAMIC PITCH-DAMPING DERIVATIVES AS MEASURED BY A FORCED-OSCILLATION BALANCE FOR PRELIMINARY VIKING CONFIGURATIONS

J. P. Billingsley and W. S. Norman
ARO, Inc.

Approved for public release; distribution unlimited

FOREWORD

This technical report has been reviewed and is approved.

Emmett A. Niblack, Jr   Frank J. Passarello
Lt Colonel, USAF   Colonel, USAF
AF Representative, VKF   Acting Director
Directorate of Test   Directorate of Test

DOCUMENT CONTROL DATA - R & D

(Security classification of title, body of abstract and indexing annotation must be entered when the overall report is classified)

1 ORIGINATING ACTIVITY (Corporate author)	2a. REPORT SECURITY CLASSIFICATION
Arnold Engineering Development Center	UNCLASSIFIED
Arnold Air Force Station, Tennessee 37389	2b GROUP N/A

3 REPORT TITLE

RELATIONSHIP BETWEEN LOCAL AND EFFECTIVE AERODYNAMIC PITCH-DAMPING DERIVATIVES AS MEASURED BY A FORCED-OSCILLATION BALANCE FOR PRELIMINARY VIKING CONFIGURATIONS

4 DESCRIPTIVE NOTES (Type of report and inclusive dates)

Final Report - May 1 through November 1, 1971

5 AUTHOR(S) (First name, middle initial, last name)

J.P. Billingsley and W.S. Norman, ARO, Inc.

6 REPORT DATE	7a TOTAL NO OF PAGES	7b NO OF REFS
May 1972	50	10

8a CONTRACT OR GRANT NO	9a ORIGINATOR'S REPORT NUMBER(S)
b PROJECT NO	
	AEDC-TR-72-25
c Program Element 921E	9b OTHER REPORT NO(S) (Any other numbers that may be assigned this report)
d	ARO-VKF-TR-71-229

10 DISTRIBUTION STATEMENT

Approved for public release; distribution unlimited.

11 SUPPLEMENTARY NOTES	12 SPONSORING MILITARY ACTIVITY
Available in DDC.	NASA, Langley Research Center Langley AFB, VA 32265

13 ABSTRACT

     Forced-oscillation pitch-damping balances oscillate over a small angular amplitude range about a nominal angle of attack and thus yield an effective value of the aerodynamic damping if the damping is a nonlinear function of angle of attack. Because the local value of the damping coefficient is generally required for computer-simulated motion studies, a procedure to extract the local damping from the experimental effective damping output of a forced-oscillation balance is derived. A derivation is given of the basic integral equation relating local and effective damping. Techniques for solving this integral equation are given. The method is applied to experimental nonlinear damping data for three preliminary unmanned Mars reentry (Viking) configurations, and the results are discussed.

DD FORM 1473
1 NOV 65

14 KEY WORDS	LINK A		LINK B		LINK C	
	ROLE	WT	ROLE	WT	ROLE	WT
VIKING spacecraft wind tunnel testing aerodynamic characteristics testing techniques balances mechanical damping						

AFSC
Arnold AFS Tenn

ABSTRACT

Forced-oscillation pitch-damping balances oscillate over a small angular amplitude range about a nominal angle of attack and thus yield an effective value of the aerodynamic damping if the damping is a nonlinear function of angle of attack Because the local value of the damping coefficient is generally required for computer-simulated motion studies a procedure to extract the local damping from the experimental effective damping output of a forced-oscillation balance is derived. A derivation is given of the basic integral equation relating local and effective damping. Techniques for solving this integral equation are given The method is applied to experimental nonlinear damping data for three preliminary unmanned Mars reentry (Viking) configurations, and the results are discussed.

CONTENTS

NOMENCLATURE

A_k k^{th} Fourier coefficient for C_{m_D}, Eq. (33) and Fig. 5

a_k k^{th} Fourier coefficient for $C_{m_{D_{eff}}}$, Eq. (33) and Fig 5

B_α Balance flexure spring constant, ft-lb/rad

$B_\alpha^\cdot$ Balance damping tare, ft-lb-sec/rad

b Slope defined by Eq. (61), per rad

C_0-C_8 Coefficients in the polynomial representation of C_{m_D} and $C_{m_{D_{eff}}}$ (Eqs (34) and (39))

C_m Pitching-moment coefficient, pitching moment/$q_\infty Sd$

C_{m_D} $C_{m_q} + C_{m_{\dot\alpha}}$, per rad

C_{m_α} $\partial C_m/\partial\alpha$, per rad

$C_{m_{\dot\alpha}}$ $\partial C_m/\partial(\dot\alpha d/2V_\infty)$, per rad

C_{m_q} $\partial C_m/\partial(qd/2V_\infty)$, per rad

d   Maximum model diameter, ft

EVENS   Defined by Eq. (35)

I   Model moment of inertia about pivot axis, ft-lb-sec/rad

i,j,k   General subscripts and indices

ℓ Model length, ft

M_a Total aerodynamic moment, Eq (20), ft-lb

M_a' Defined by Eq. (17), ft-lb

M_D $M_q + M_{\dot\alpha}$, ft-lb-sec/rad

M(t)   Forcing moment of balance, ft-lb

M_h Hysteresis moment, ft-lb (Eq (28))

M_∞ Free-stream Mach number

M_α Aerodynamic pitching-moment slope, $q_\infty Sd\ C_{m_\alpha}$, ft-lb/rad

$M_{\dot\alpha}$ $[(q_\infty Sd^2)/(2V_\infty)]\ C_{m_{\dot\alpha}}$, ft-lb-sec/rad

M_q $[(q_\infty Sd^2)/(2V_\infty)]\ C_{m_q}$, ft-lb-sec/rad

M_T Sum of aerodynamic, balance flexure, and forcing moments acting on model, ft-lb (Eqs (1) and (2))

N   Indices for α where $C_{m_D} = C_{m_{D_{eff}}}$ (Fig 4)

ODDS   Defined by Eq (36)

P_1-P_8 Defined by Eqs (49) through (56), respectively

q   Pitching rate, in general, and $\dot\alpha$, in particular, for the balance, rad/sec

q_∞ Free-stream dynamic pressure, lb/ft^2

R_0-R_8 Defined by Eqs. (40) through (48), respectively

Re_d Free-stream Reynolds number based on model maximum diameter

S Reference area, $\pi d^2/4$, ft^2

t Time, sec

T_k k^{th} coefficient in series representation of M(t) ft-lb

V_∞ Free-stream velocity, ft/sec

W_k k^{th} weighting function relating A_k to a_k, Eq. (33)

x_{cg} Model center of gravity location with respect to nose, in. (Fig. 9)

a Instantaneous angle of attack of model, rad

a_E Defined in Fig. 8, rad

a_{max} a limit in Fourier series representation of C_{m_D}, rad (Fig. 5)

a_N a where $C_{m_D} = C_{m_{D_{eff}}}$ (see Fig. 4), rad

a_o Nominal or equilibrium angle of attack, Eq. (4), rad

a_{ST} Balance sting angle of attack, rad

$\dot{a}$ Time rate of change of angle of attack, rad/sec

β Integral limit defined by Eq (37), rad

$\gamma_1, \gamma_2, \gamma_3,$ Integral limits defined by Eqs. (57), (58), and (59), respectively, rad (Fig. 8)

Δa Increment of a defined in Fig 4, rad

θ Instantaneous angular oscillation position, rad

$\dot{\theta}$ Time rate of change of θ, rad/sec

θ_1 Maximum angular oscillation amplitude for a cycle of motion, rad

$\theta_0, \theta_1, \theta_e$ Defined in Fig. 2, rad

φ Phase angle between forcing moment, M(t), and oscillation amplitude, $\theta(t)$, rad

ω Angular circular frequency of M(t) or θ(t), rad/sec

ω_N Natural circular frequency of balance system $\sqrt{-(M_a + B_a)/I}$, rad/sec

SUBSCRIPTS

eff   Effective value

ST   Sting

SECTION I
INTRODUCTION

Two general procedures are available for measuring pitch-damping dynamic stability coefficients for a captive (sting-supported) model in a wind tunnel (Ref 1) These methods are the forced-oscillation and the free-oscillation techniques The free-oscillation balance is usually somewhat simpler in design and operation than a forced-oscillation balance, but the forced-oscillation balance provides more precise control of the amplitude of the oscillation, which can be particularly important if the model is dynamically unstable Data reduction for a forced-oscillation system is generally simpler than for a free-oscillation balance. The free-oscillation balance yields transient angular motion data which must be analyzed in terms of the decay in the amplitude to yield the desired damping coefficients As described below, the forced-oscillation balance operates at constant angular motion, and the damping coefficients are obtained directly from the torque input measurements

The von Kármán Gas Dynamics Facility (VKF) of the Arnold Engineering Development Center (AEDC) has developed a forced-oscillation dynamic balance to measure pitch (or yaw) damping. This balance is sting supported with a cross-flexure spring pivot system which allows one degree of freedom in angular motion The balance system is described in Refs. 1 and 2. Certain essential features of the system operation are also described herein to provide the necessary background for the present analysis A schematic representation of the VKF forced-oscillation balance is depicted in Fig 1

The balance is equipped with a magnetic shaker motor and feedback control (Fig 2) to provide oscillation amplitudes, θ_1, from essentially zero to approximately 2 deg However, to reduce effects of tunnel vibrations, it is generally necessary to make the oscillation amplitude greater than about 1 deg The balance system output is a damping coefficient which is the mean value over a cycle of motion for that particular oscillation amplitude, θ_1, at the nominal angle of attack, a_o. As the oscillation amplitude is lowered, the "effective" damping determined by the system approaches the "local" value for that particular a_o. If the damping coefficient is a linear function of a within the region $a_o + \theta_1$ to $a_o - \theta_1$, then the balance system gives the true local value of the damping coefficient on that particular a_o.

The values of the damping coefficient obtained from the forced-oscillation technique are easily interpreted if the variation of the local value of the damping coefficient with angle of attack is small within the range covered during the oscillation from $a_o - \theta_1$ to $a_o + \theta_1$. There exist cases for which the variation of damping coefficient over the range of angle of attack is quite large. One such case was the unmanned Mars landing vehicle (Viking), tested in the AEDC Propulsion Wind Tunnels (Refs 3 and 4), which was found to be dynamically unstable for small angles of attack (less than about 2 deg) and dynamically stable at higher angles. The variation of the damping coefficient with angle of attack over the angle-of-attack range covered in the forced oscillation was quite large. The purpose of this report is to describe the mathematical techniques by which the value of the damping coefficients for very small oscillations (termed the local value, $C_{m_D}(a_o)$) can be determined from the effective value obtained with the forced oscillation

Fig. 1 Schematic Representation of Balance System
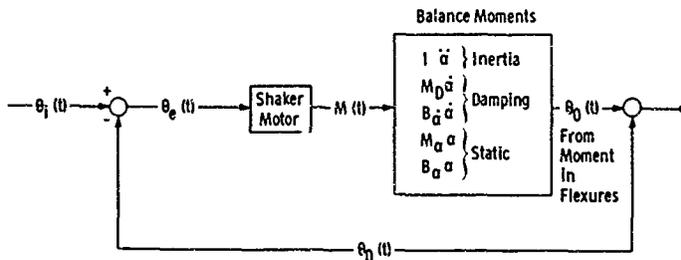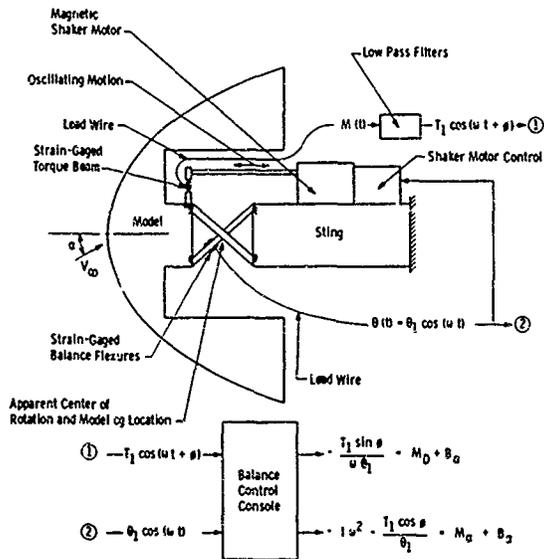
$\theta_0 (t)$ — Actual Output from Flexures

$\theta_i (t)$ — Desired Output from Flexures = $\theta_1 \cos \omega t$

$\theta_e (t)$ — Error Signal = $\theta_i (t) - \theta_0 (t)$

Fig. 2 Schematic of Balance Feedback Control System

2

balance by oscillating the system with an amplitude, θ_1, about the angle of attack a_o, $C_{m_{D_{eff}}} (a_o, \theta_1)$ As the value of θ_1 goes to zero, the effective value and the local value are the same; i e.,

$$\theta_1 \lim_{\longrightarrow} 0 \, C_{m_{D_{eff}}} (a_o, \theta_1) = C_{m_D}(a_o)$$

The local damping coefficients are of practical importance because they are required in computer simulations of dynamic motions.

SECTION II
ANALYSIS

2.1 FORCED-OSCILLATION BALANCE SYSTEM OUTPUT

A schematic of the VKF forced-oscillation balance is shown in Fig. 1 A magnetic shaker motor is used to impose an approximately sinusoidal oscillation upon the model The moments opposing the moment input by the motor are those attributable to inertia, the aerodynamic restoring moment, and the flexure. Strain gages are attached to the input torque beam and the flexure. The first of these gives the input moment from the shaker motor, and the second is used to determine the angular position of the model, θ.

A feedback into the shaker motor control is used to maintain the amplitude of the model oscillation, θ_1, at a preselected value (Fig. 2). It is this feedback that allows the device to be used even with dynamically unstable systems since, for these, the shaker motor extracts energy from the system being tested With a dynamically stable system, the shaker motor must add energy to the system to maintain a constant amplitude.

To determine the damping, the frequency is varied until a phase shift, ϕ, of approximately 90 deg between the input torque and the displacement, θ, is obtained At this condition the moments attributable to inertia and stiffness are essentially in balance, so the output of the shaker motor is basically compensating for the damping moment. The amplitudes of the moment, T_1, and the displacement, θ_1, along with the frequency, ω, allow the damping term to be evaluated

The control console is shown schematically in the lower portion of Fig. 1. Internally, there are low pass filters, phase shifters, and multipliers, which are used to give the amplitudes of the in-phase and out-of-phase components of the input torque From these the aerodynamic damping and stiffness may be determined.

The basic differential equation for a forced-oscillation pitch-damping balance is

$$I\ddot{\alpha} = M_1 \tag{1}$$

$$= \underbrace{M_{D}\dot{\alpha} + M_{\alpha}\alpha}_{\substack{\text{Aerodynamic} \\ \text{Restoring Moment}}} + \underbrace{B_{\dot{\alpha}}\dot{\alpha} + B_{\alpha}(\alpha - \alpha_{\searrow 1})}_{\substack{\text{Balance Flexure} \\ \text{Moment}}} + \underbrace{M(t)}_{\substack{\text{Forcing Moment} \\ \text{of Shaker}}} \tag{2}$$

3

in which

I = Model moment of inertia about pivot axis

M_T = Sum of aerodynamic, balance flexure, and forcing moments acting on model about pivot axis

M_D = Aerodynamic damping moment per angular velocity
$= (C_{m_{\dot{\alpha}}} + C_{m_q})\, q_\infty S d^2 / 2V_\infty$

M_α = Aerodynamic pitching moment per unit angle (stiffness)
$= C_{m_\alpha}\, q_\infty S d$

$B_{\dot{\alpha}}$ = Balance flexure structural damping moment per angular velocity

B_α = Balance flexure moment per unit angle (stiffness)

$M(t)$ = Forced oscillatory moment impressed on model

α_{ST} = Stationary angle of attack of sting

α = Instantaneous angle of attack of the model

The angle of attack may be written as

$$\alpha = \alpha_o + \theta(t) \tag{3}$$

where

$\theta(t)$ = Instantaneous oscillation amplitude about α_o

α_o = Equilibrium angle of attack of model

The relation between the sting angle and the equilibrium angle is given by

$$\alpha_o = \frac{B_\alpha}{B_\alpha + M_\alpha}\, \alpha_{ST} \tag{4}$$

The relationships among the various angles are shown in Fig. 3.

After substituting Eqs. (2), (3), and (4) into Eq (1), the basic balance equation becomes

$$I\ddot{\theta} - (M_D + B_{\dot{\alpha}})\dot{\theta} - (M_\alpha + B_\alpha)\theta = M(t) \tag{5}$$

4
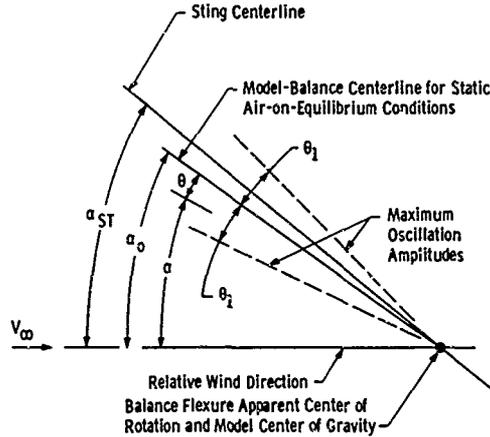
Fig. 3 Geometry of Pitch-Damping Balance-Sting Combination

The stiffness of the flexure, B_a, is generally selected to be much greater than the aerodynamic stiffness, M_a, since the latter varies widely with tunnel conditions. This also decreases the effects of nonlinearities in the static restoring moment. In addition, the system is designed so that B_a is constant over the range of deflections encountered. This, in conjunction with the feedback control system, permits the oscillation amplitude to be accurately represented by a pure cosine wave

$$\theta(t) = \theta_1 \cos \omega t \tag{6}$$

The output of the torque beam will, in general, contain higher harmonics, since by Eq. (5) all the damping and nonlinear terms will be included in M(t). Thus, the input moment can be expressed in a Fourier series

$$M(t) = I\ddot{\theta} - (M_b + B_a)\theta - (M_a + B_a)\theta$$
$$= \sum_{k=1}^{\infty} T_k \cos (k\omega t + \phi) \tag{7}$$

If all of the coefficients in the basic differential equation are constants, then only the first term ($k = 1$) is present in M(t). Using Eq. (6) and collecting the coefficients of cos ωt (in phase) and sin ωt (out of phase) give for this particular case

$$- I\omega^2\theta_1 - (M_a + B_a)\theta_1 = T_1 \cos \phi$$
$$- (M_b + B_a)\omega\theta_1 = T_1 \sin \phi \tag{8}$$

5

Thus

$$M_\alpha + B_\alpha = -I\omega^2 - \frac{T_1}{\theta_1} \cos \phi \qquad (9)$$

equals total static moment slope, and

$$M_D + B_{\dot\alpha} = -\frac{T_1 \sin \phi}{\omega\theta_1} \qquad (10)$$

equals total system damping coefficient.

Normally the frequency is selected ($\omega = \omega_N$) to give a phase shift of 90 deg in order to maximize the accuracy with which the damping coefficient may be determined.

The measured values of T_1, ϕ, ω, and θ_1, and values of B_α and $B_{\dot\alpha}$ from pretest calibrations then allow the aerodynamic coefficients, M_α and M_D, to be determined from Eqs. (9) and (10). Normally, the aerodynamic stiffness, M_α, may be determined more accurately with a static balance. The aerodynamic damping, M_D, is the sum of $M_{\dot\alpha}$ and M_q. The individual contributions of $M_{\dot\alpha}$ and M_q cannot be distinguished by the balance, since $\dot\alpha$ = q for the balance.

2.2 EQUIVALENT DAMPING FOR NONLINEAR SYSTEMS

If there are nonlinearities in the system, either or both of the coefficients M_D and M_α may vary. In general, each may be a function of α and $\dot\alpha$. To avoid certain pitfalls, it is preferable to begin with the expression for the total aerodynamic moment, M_a, as a function of α and $\dot\alpha$

$$M_a = M_a(\alpha, \dot\alpha) \qquad (11)$$

The circuitry of the console contains low-pass filters so that the higher harmonics of M(t) are filtered out. Therefore, the system gives the fundamental harmonic; i.e., the in-phase ($T_1 \cos \phi$) and the out-of-phase ($T_1 \sin \phi$) fundamental components of the input torque. In general

$$M(t) = I\ddot\theta - B_{\dot\alpha}\dot\theta - B_\alpha\theta - M_a(\alpha_o + \theta, \dot\theta)$$

$$= \sum_{k=1}^{\infty} T_k \cos (k\omega t + \phi) \qquad (12)$$

and

$$T_1 \cos \phi = \frac{1}{\pi} \int_0^{2\pi} M(t) \cos \omega t \, d(\omega t) \qquad (13)$$

$$-T_1 \sin \phi = \frac{1}{\pi} \int_0^{2\pi} M(t) \sin \omega t \, d(\omega t) \qquad (14)$$

6

With $\theta = \theta_1 \cos \omega t$ these become

$$T_1 \cos \phi = \frac{1}{\pi} \int_0^{2\pi} [- I\omega^2 \theta_1 \cos \omega t + B_{\dot{\alpha}} \omega \theta_1 \sin \omega t - B_\alpha \theta_1 \cos \omega t - M_a'] \cos \omega t \, d(\omega t) \quad (15)$$

$$-T_1 \sin \phi = \frac{1}{\pi} \int_0^{2\pi} [- I\omega^2 \theta_1 \cos \omega t + B_{\dot{\alpha}} \omega \theta_1 \sin \omega' - B_\alpha \theta_1 \cos \omega t - M_a'] \sin \omega t \, d(\omega t) \quad (16)$$

with

$$M_a' = M_a(a_0 + \theta_1 \cos \omega t, - \omega \theta_1 \sin \omega t) \quad (17)$$

Certain of the integrals may be evaluated, with the result

$$T_1 \cos \phi = - I\omega^2 \theta_1 - B_\alpha \theta_1 - \frac{1}{\pi} \int_0^{2\pi} M_a(a_0 + \theta_1 \cos \omega t_1, -\omega \theta_1 \sin \omega t) \cos \omega t \, d(\omega t) \quad (18)$$

$$-T_1 \sin \phi = B_{\dot{\alpha}} \omega \theta_1 - \frac{1}{\pi} \int_0^{2\pi} M_a(a_0 + \theta_1 \cos \omega t, - \omega \theta_1 \sin \omega t) \sin \omega t \, d(\omega t) \quad (19)$$

These results are valid for arbitrary aerodynamic moments.

It is of interest to simplify these results for certain specific cases If the aerodynamic moment is a continuous function of the angular velocity, then an expansion can be made about an angular velocity of zero.

$$M_a(a, \dot{a}) = M_a(a, 0) + \frac{\partial M_a}{\partial \dot{a}}(a, 0)\dot{a} + \frac{1}{2} \frac{\partial^2 m_a}{\partial \dot{a}^2}(\dot{a}, 0)\dot{a}^2 + \dots \quad (20)$$

In terms of these quantities

$$M_\alpha = M_a(a, 0) \, \alpha \quad (21)$$

$$M_D = \frac{[M_a(a, \dot{a}) - M_a(a, 0)]}{\dot{a}}$$

$$= \frac{\partial M_a}{\partial \dot{a}}(a, 0) + \frac{1}{2} \frac{\partial^2 M_a}{\partial \dot{a}^2}(a, 0)\dot{a} + \dots \quad (22)$$

7

The parameter M_α is therefore independent of velocity. This is a direct consequence of the assumption that M_s is continuous, since any dependence upon velocity appears in M_D. The moment can now be written as

$$M_s(\alpha, \dot{\alpha}) = M_\alpha(\alpha)\alpha + M_D(\alpha, \dot{\alpha})\dot{\alpha} \tag{23}$$

With this representation, the integrals may be simplified

$$\frac{T_1 \cos \phi}{\theta_1} = -I\omega^2 - B_\alpha - \frac{1}{\pi\theta_1}\int_0^{2\pi} M_\alpha(\alpha)\alpha \, \cos \omega t \, d(\omega t)$$

$$= -I\omega^2 - B_\alpha - \frac{\omega}{\pi}\int_0^{2\pi} M_\alpha(\alpha_0 + \theta_1 \cos \omega t) \cos^2 \omega t \, d(\omega t) \tag{24}$$

$$-\frac{T_1 \sin \phi}{\omega\theta_1} = B_{\dot{\alpha}} + \frac{1}{\pi}\int_0^{2\pi} M_D(\alpha_0 + \theta_1 \cos \omega t, \, -\omega\theta_1 \sin \omega t) \sin^2 \omega t \, d(\omega t) \tag{25}$$

According to this, nonlinearities in the static moment do not affect the damping as determined by the forced-oscillation balance. This is valid if M_s is a single valued function of α.

If the damping coefficient is expanded in terms of $\dot{\alpha}$, i.e.

$$M_D(\alpha, \dot{\alpha}) = M_D(\alpha, 0) + \frac{\partial M_D}{\partial \dot{\alpha}}(\alpha, 0)\dot{\alpha} + \frac{1}{2}\frac{\partial^2 M_D}{\partial \dot{\alpha}^2}(\alpha, 0)\dot{\alpha}^2 \tag{26}$$

Equation (25) becomes

$$-\frac{T_1 \sin \phi}{\omega\theta_1} = B_{\dot{\alpha}} + \frac{1}{\pi}\int_0^{2\pi} M_D(\alpha_0 + \theta_1 \cos \omega t, 0) \sin^2 \omega t \, d(\omega t)$$

$$+ \frac{\omega^2\theta_1^2}{\pi}\int_0^{2\pi} \frac{\partial^2 M_D}{\partial \dot{\alpha}^2}(\alpha_0 + \theta_1 \cos \omega t, 0) \sin^4 \omega t \, d(\omega t) \tag{27}$$

$$+ \frac{\omega^4\theta_1^4}{\pi}\int_0^{2\pi} \frac{\partial^4 M_D}{\partial \dot{\alpha}^4}(\alpha_0 + \theta_1 \cos \omega t, 0) \sin^6 \omega t \, d(\omega t) + \ldots$$

The left-hand side of this equation is the value determined by the forced-oscillation technique. If the aerodynamic damping coefficient M_D is constant or is a linear function of $\dot{\alpha}$, then the result reverts to that given by Eq. (10). If the aerodynamic coefficient is nonlinear with angular velocity, i.e.

$$\frac{\partial^2 M_D}{\partial \dot{\alpha}^2} \neq 0$$

8

according to Eq. (27) the apparent effective damping determined by the forced-oscillation technique will depend upon the frequency, ω. For this reason it is advisable to obtain data at two or more frequencies, which requires using more than one set of flexures If there is no dependence upon frequency noted, then it may be concluded that

$$\frac{\partial^{2n}M_D}{\partial\dot{a}^{2n}} = 0$$

One class of nonlinearities that does not fall within the above framework is hysteresis, because the moment is not a continuous analytic function of velocity. If M_h is the hysteresis moment, and assuming for simplicity that the variation of M_a with a is linear

$$\begin{aligned} M_a &= M_\alpha a + M_h & \dot{a} > 0 \\ &= M_\alpha a - M_h & \dot{a} < 0 \end{aligned} \tag{28}$$

Then

$$\frac{T_1 \sin\theta}{\omega\theta_1} = B_\alpha + \frac{4}{\pi}\frac{M_h}{\omega\theta_1} \tag{29}$$

In this case the apparent damping varies inversely with $\omega\theta_1$. Since the balances operate at constant $\omega\theta_1$, the quantity $(4M_h/\pi\omega\theta_1)$ would appear to the balance system as a constant value of effective aerodynamic damping, $M_{D_{eff}}$, for that particular test condition. As with the case of a nonlinear damping coefficient, testing at different frequencies would reveal the existence of the effect.

In the remaining development it is assumed that there is no hysteresis, and the nonlinearities with respect to angular velocity in the damping coefficient are negligible Under these conditions

$$-\frac{T \sin\phi}{\omega\theta_1} = B_\alpha + \frac{1}{\pi}\int_0^{2\pi}M_D(a_o + \theta_1 \cos\omega t, 0) \sin^2\omega t \, d(\omega t) \tag{30}$$

If now the local value of damping derivative, $C_{m_D}(a)$, is related to M_D and the effective value, $C_{m_{D_{eff}}}(a_o, \theta_1)$, is that determined from the forced-oscillation technique, i e, from Eq. (30), then

$$C_{M_{D_{eff}}}(a_o,\theta_1) = \frac{1}{\pi}\int_0^{2\pi}C_{M_D}(a_o + \theta_1 \cos\omega t) \sin^2\omega t \, dt \tag{31}$$

Equation (31) is an integral equation which relates the effective experimental damping obtained from the present balance system to the local damping This integral relationship can also be obtained directly, without considering the balance output, by equating the amount of energy dissipated per cycle by the local and effective damping (Refs 5, 6, and 7).

9

Equation (31) is valid for a nonlinear pitching moment (C_m versus a) so long as the pitching moment is single valued for a given a. That is, pitching-moment hysteresis or time lags (because of viscous effects) can also add or dissipate system energy, which will then appear as nonlinear damping (Eq (29)).

2.3 SOLUTION OF INTEGRAL EQUATION

Equation (31) is a Fredholm integral equation of the first kind (Ref. 8). The known quantity is $C_{m_{D_{eff}}}$ which is a function of a_o and θ_1 and usually is known for various values of a_o at a fixed value of θ_1. The unknown quantity is C_{m_D}, which is a function of a. Three ways of solving this equation were tried, with the first two being unsuccessful.

For the first approach, Eqs. (3) and (6) were used in Eq (31) to give

$$C_{M_{D_{eff}}}(a_o, \theta_1) = \frac{2}{\pi \theta_1} \int_{a_o - \theta_1}^{a_o + \theta_1} C_{M_D}(a) \sqrt{1 - \left(\frac{a - a_o}{\theta_1}\right)^2} \, da \qquad (32)$$

Equation (32) was written in finite difference form involving the known values of $C_{m_{D_{eff}}}$ and the unknown values of C_{m_D} (Fig. 4) The procedure was very similar to that mentioned in Ref. 9. This formulation led to a set of linear simultaneous equations for the unknown quantities which could be solved by standard techniques. The answers, however, were extremely sensitive to the input values of the effective damping. The results, in general, were very erratic, even for simple test cases, and the method was abandoned.

The second approach to obtain a practical relationship between the local and effective damping consisted of a series solution for Eq. (32) (Ref. 8) The known effective damping and the unknown local damping were represented by Fourier cosine series. The kernel was represented by various types of power series in a. This allowed the analytic evaluation of the integral for a general term, and a relation between the known (effective) and unknown (local) Fourier coefficients could be established. This relation for the kth coefficient is of the form

$$A_k = \frac{a_k}{W_k} \qquad (33)$$

The weighting coefficient, W_k, is shown schematically in Fig. 5 as a function of k. Note that for large values of k, W_k is very small and oscillates about zero. It was this oscillatory behavior of W_k that led to the abandonment of this method, since Eq. (33) could become singular unless a_k was determined from "mathematically perfect" data for $C_{m_{D_{eff}}}$. This basic procedure has been proposed (but not applied) recently in Ref 10, where W_k is evaluated by Bessel functions. Unfortunately, the method places such a premium on the quality of the input data and the Fourier series representation of this data that it is not practical for this particular case.

10
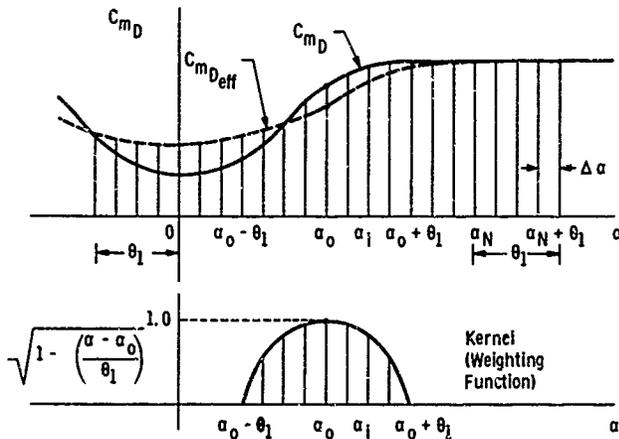
$$C_{m_{D_{eff}}} (\alpha_j, \theta_1) = \frac{2}{\pi \theta_1} \left[\sum_{i=j-k}^{i=j+k} C_{m_D}(\alpha_i) \sqrt{1 - \left(\frac{\alpha_i - \alpha_0}{\theta_1}\right)^2} \, \Delta\alpha \right]_j$$

$j = 1--N, \quad \alpha_0 = j\Delta\alpha, \quad \theta_1 = k\Delta\alpha$

This provides N linear equations which may be solved for N unknown values of C_{m_D}.

Fig. 4 Schematic Illustration of the Damping in Discrete Variable Form

11

$$C_{m_{D_{eff}}} = \frac{a_0}{2} + \sum_{k=1}^{N} a_k \cos \left(\frac{k \pi \alpha}{\alpha_{max}}\right) d\alpha$$

$$C_{m_D} = \frac{A_0}{2} + \sum_{k=1}^{N} A_k \cos \left(\frac{k \pi \alpha}{\alpha_{max,}}\right) d\alpha$$

$$a_k = \frac{2}{\alpha_{max}} \int_0^{\alpha_{max}} C_{m_{D_{eff}}} (\alpha) \cos \left(\frac{k \pi \alpha}{\alpha_{max}}\right) d\alpha$$

$$A_k = \frac{2}{\alpha_{max}} \int_0^{\alpha_{max}} C_{m_D} (\alpha) \cos \left(\frac{k \pi \alpha}{\alpha_{max}}\right) d\alpha$$

$$= \frac{a_k}{W_k}$$
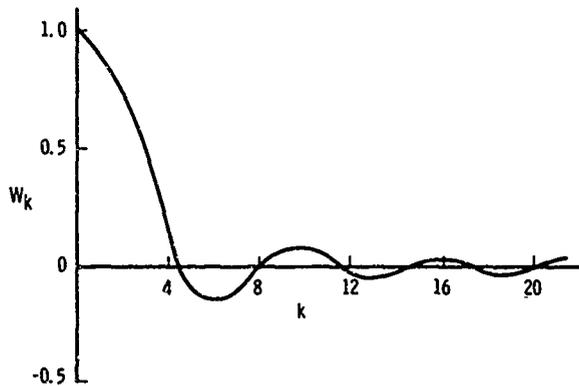
Fig. 5 Typical Variation of W_k versus k

12

Both of the above techniques failed because of a very strong sensitivity of the local damping coefficient to the effective damping coefficient. Many physically unrealistic values of the local damping coefficient were obtained, such as values that were alternately large positive and large negative. The reason for this behavior can be seen in Fig 5, which essentially states that there are certain specific values of higher frequency contribution which should not be present in the effective damping. Because of noise and other inaccuracies, such frequencies will be present, and, in the inversion process, effects of the noise will dominate.

To overcome this undesirable effect, smoothing of the input data is necessary In the second approach smoothing by Fourier series was found to be unacceptable The hird approach made use of polynomial smoothing. The manner in which this was accomplished is somewhat similar to the procedure given in Ref. 6 for free-oscillation pitch-damping data. However, certain features of the present analysis for forced oscillation were not necessary in Ref. 6 and, as such, merit inclusion here. To provide continuity, the procedure is outlined in detail

It is assumed that C_{m_D} can be represented by a power series in α of the form

$$C_{M_D} = C_0 + C_1|\alpha| + C_2\alpha^2 + C_3|\alpha|^3 + C_4\alpha^4 + C_5|\alpha|^5 + C_6\alpha^6 + C_7|\alpha|^7 + C_8\alpha^8 \quad (34)$$

The odd powers are included to enhance the curve fitting capability, but they must be considered as absolute quantities because of the requirement that C_{m_D} be symmetrical about an angle of attack of zero. This is valid for a body of revolution

Equations (3) and (6) are substituted into Eq (34). The resulting expression for C_{m_D} may be substituted into Eq (30) and integrated analytically. It is convenient to work with the even and odd terms separately The even terms of Eq (34) are

$$\text{EVENS} = C_0 + C_2(\alpha_0 + \theta_1 \cos \omega t)^2 + C_4(\alpha_0 + \theta_1 \cos \omega t)^4 \\ + C_6(\alpha_0 + \theta_1 \cos \omega t)^6 + C_8(\alpha_0 + \theta_1 \cos \omega t)^8 \quad (35)$$

The odd terms of Eq. (34) are

$$\text{ODDS} = C_1(\alpha_0 + \theta_1 \cos \omega t) + C_3(\alpha_0 + \theta_1 \cos \omega t)^3 \\ + C_5(\alpha_0 + \theta_1 \cos \omega t)^5 + C_7(\alpha_0 + \theta_1 \cos \omega t)^7 \quad (36)$$

If α_0 is less than θ_1, then α will be negative over a portion of the half cycle (Figs 6 and 7). Again referring to Figs. 6 and 7 and using Eqs. (3) and (6), β can be determined

$$0 = \alpha_0 + \theta_1 \cos(\pi - \beta)$$

$$\beta = \arccos \frac{\alpha_0}{\theta_1} \qquad \alpha_0 \leq \theta_1 \qquad (37)$$

$$\beta = 0 \qquad \qquad \alpha_0 > \theta_1$$

13
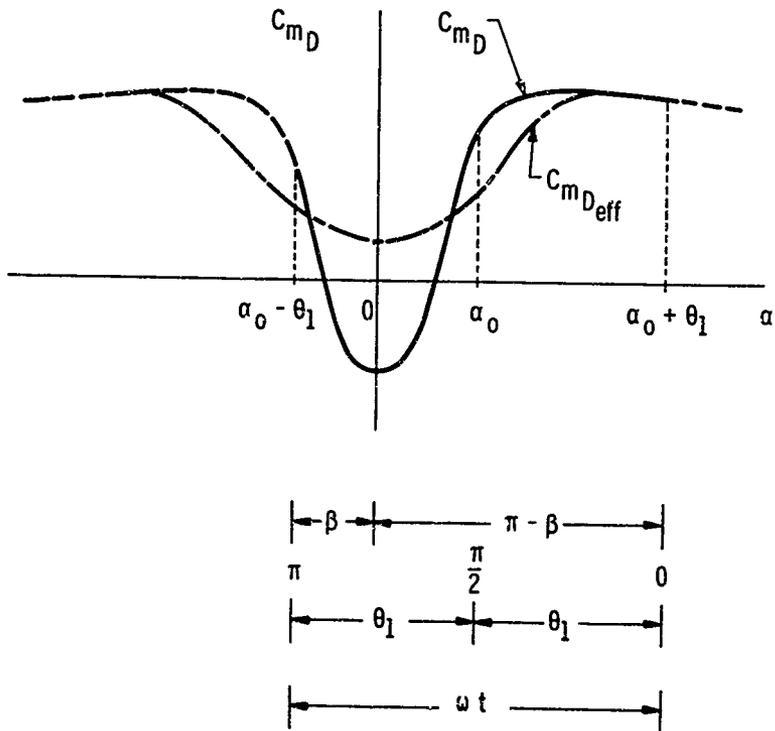
Fig. 6 Schematic Depiction of Integral Limits for Polynomial Representation
of Damping
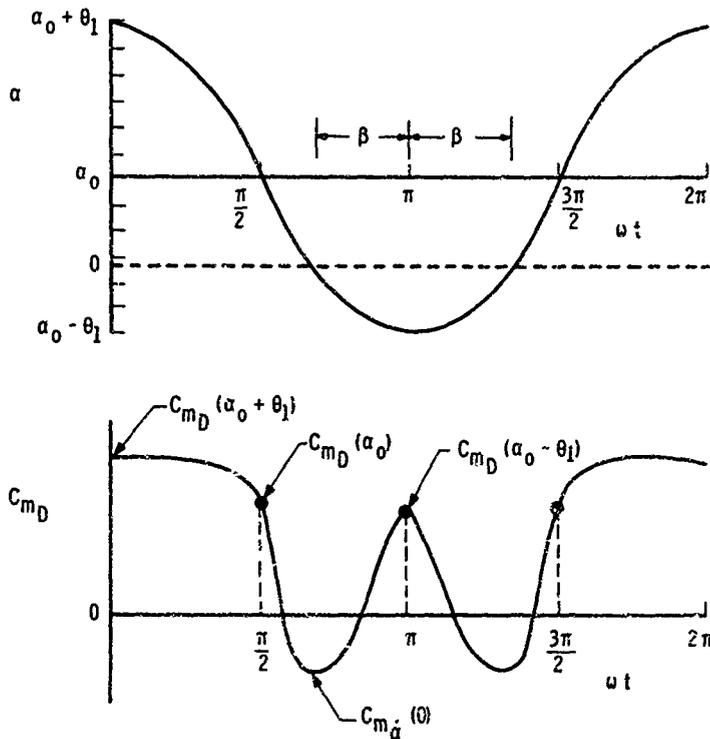
Fig. 7 Typical Cyclic Variation of α and C_{m_D}

The odd terms are made positive (or absolute) in the cyclic region from $\pi - \beta$ to π by changing sign. With reference to Fig. 7 and Eq. (31), the same amounts of energy are dissipated over each half cycle. Consequently, Eqs. (35), (36), and the results of Eq. (37) can be combined with Eq. (31) to give

$$C_{m_{D_{eff}}} = \frac{2}{\pi} \int_{0}^{\pi} \{EVENS\} \sin^2(\omega t)\, d(\omega t)$$

$$+ \frac{2}{\pi} \int_{0}^{\pi-\beta} \{ODDS\} \sin^2(\omega t)\, d(\omega t) \tag{38}$$

$$- \frac{2}{\pi} \int_{\pi-\beta}^{\pi} \{ODDS\} \sin^2(\omega t)\, d(\omega t) \quad .$$

The evaluation of Eq. (38) yields

$$C_{m_{D_{eff}}} = C_0 R_0 + C_1 R_1 \quad C_2 R_2 + C_3 R_3 + C_4 R_4$$
$$+ C_5 R_5 + C_6 R_6 + C_7 R_7 + C_8 R_8 \tag{39}$$

where

$$R_0 = 1.0 \tag{40}$$

$$R_1 = p_1 a_o + \frac{2}{3} p_2 \theta_1 \tag{41}$$

$$R_2 = a_o^2 + \frac{1}{4} \theta_1^2 \tag{42}$$

$$R_3 = p_1 a_o^3 + 2p_2 a_o^2 \theta_1 + \frac{3}{4} p_3 a_o \theta_1^2 + 2p_4 \theta_1^3 \tag{43}$$

$$R_4 = a_o^4 + \frac{3}{2} a_o^2 \theta_1^2 + \frac{1}{8} \theta_1^4 \tag{44}$$

$$R_5 = p_1 a_o^5 + \frac{10}{3} p_2 a_o^4 \theta_1 + \frac{5}{2} p_3 a_o^3 \theta_1^2 + 20 p_4 a_o^2 \theta_1^3 + \frac{5}{8} p_5 a_o \theta_1^4 + 2p_6 \theta_1^5 \tag{45}$$

$$R_6 = a_o^6 + \frac{15}{4} a_o^4 \theta_1^2 + \frac{15}{8} a_o^2 \theta_1^4 + \frac{5}{64} \theta_1^6 \tag{46}$$

$$R_7 = p_1 a_o^7 + \frac{14}{3} p_2 a_o^6 \theta_1 + \frac{21}{4} p_3 a_o^5 \theta_1^2 + 70 p_4 a_o^4 \theta_1^3 + \frac{35}{8} p_5 a_o^3 \theta_1^4$$
$$+ 42 p_6 a_o^2 \theta_1^5 + \frac{35}{64} p_7 a_o \theta_1^6 + \frac{4}{3} p_8 \theta_1^7 \tag{47}$$

$$R_8 = a_o^8 + 7 a_o^6 \theta_1^2 + \frac{35}{4} a_o^4 \theta_1^4 + \frac{35}{16} a_o^2 \theta_1^6 + \frac{7}{128} \theta_1^8 \tag{48}$$

and

$$p_1 = \frac{2}{\pi}\left(\frac{\pi}{2} - \beta + \frac{\sin 2\beta}{2}\right) \tag{49}$$

$$P_2 \approx \frac{2}{\pi} \sin^3 \beta \tag{50}$$

$$P_3 = \frac{2}{\pi} \left(\frac{\pi}{2} - \beta + \frac{\sin 4\beta}{4} \right) \tag{51}$$

$$P_4 = \frac{2}{\pi} \left(\frac{1}{3} \sin^3 \beta - \frac{1}{5} \sin^5 \beta \right) \tag{52}$$

$$P_5 = \frac{2}{\pi} \left(\frac{\pi}{2} - \beta - \frac{\sin 2\beta}{4} + \frac{\sin 4\beta}{4} + \frac{\sin 6\beta}{12} \right) \tag{53}$$

$$P_6 = \frac{2}{\pi} \left(\frac{\sin^3 \beta}{3} - \frac{2}{5} \sin^5 \beta + \frac{\sin^7 \beta}{7} \right) \tag{54}$$

$$P_7 \approx -\frac{2}{\pi} \left(\frac{16}{5} \sin^3 \beta \cos^5 \beta \right) + P_5 \tag{55}$$

$$P_8 = \frac{2}{\pi} \left(\frac{\sin^3 \beta \cos^6 \beta}{6} \right) + P_6 \tag{56}$$

If $a_o = 0$, the above results also apply to the type of free oscillation about zero a which was considered in Ref. 6 In particular, if the odd terms are neglected for this condition, Eq. (39) reduces to Eq. (13) of Ref. 6. The polynomial method may also be applied to free-oscillation test data for a_o not equal to zero if the free-oscillation damping is determined for the same value of θ_1 from oscillation envelopes at different values of a_o.

Equation (34) (C_{m_D}) and Eq. (39) ($C_{m_{D_{eff}}}$) are related in that both contain the coefficients $C_0 ... C_8$ as unknown quantities Practical use is made of this relationship by curve-fitting the experimental values of $C_{m_{D_{eff}}}$ as functions of a_o and θ_1 with Eq (39) and determining the coefficients $C_0 ... C_8$ by a least-squares procedure. This immediately yields the corresponding values of C_{m_D} since they can now be computed from Eq (34) for a given $a = a_o$.

This analysis was made for an eighth-order polynomial curve (nine unknowns), but it is easily reduced to a sixth-order (seven unknowns) or a fourth-order (five unknowns) curve by merely deleting the higher-order terms. A program has been written for the VKF CDC-1604B computer which incorporates the above analysis relating the local and effective damping coefficients. The coefficients are determined for a minimum square-error fit to the experimental data points.

2.4 THE V-WELL AND SQUARE WELL

One of the earlier approaches to acquire insight concerning the local-effective damping relationship expressed by Eq. (31) was to assume simple variations for the local damping and compute the resulting effective damping. One such variation was the V-well representation of the local damping as depicted in Fig. 8. This simple variation is composed

17
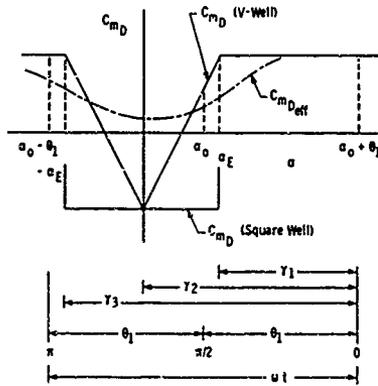
a. Schematic Depiction of Integral Limits
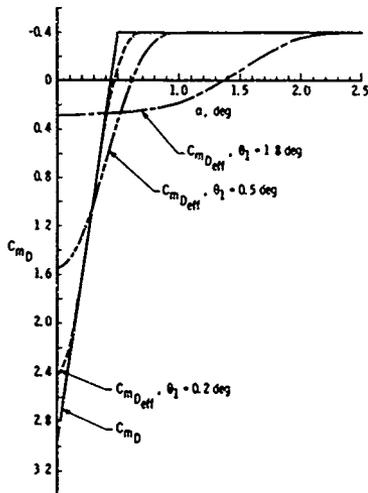
b. Typical Effect of Oscillation Amplitude on Effective Damping

Fig. 8 V-Well and Square Well Representation of Local Damping

of straight-line (linear) segments so that Eq. (31) is easy to evaluate once the proper integral limits have been established. These limits are shown schematically in Fig. 8a and are computed as follows:

$$\gamma_1 = \arccos\left[\frac{a_E - a_o}{\theta_1}\right]; \qquad \left|\frac{a_E - a_o}{\theta_1}\right| \leq 1$$

$$= 0; \qquad \left(\frac{a_E - a_o}{\theta_1}\right) > 1 \tag{57}$$

$$= \pi; \qquad \left(\frac{a_E - a_o}{\theta_1}\right) < -1$$

$$\gamma_2 = \arccos\left[\frac{-a_o}{\theta_1}\right]; \qquad \left|\frac{a_o}{\theta_1}\right| \leq 1$$

$$= \pi; \qquad \left|\frac{a_o}{\theta_1}\right| > 1 \tag{58}$$

$$\gamma_3 = \arccos\left[-\left(\frac{a_E - a_o}{\theta_1}\right)\right]; \qquad \left|\frac{a_E + a_o}{\theta_1}\right| \leq 1$$

$$= \pi; \qquad \left|\frac{a_E + a_o}{\theta_1}\right| > 1 \tag{59}$$

The V-well shape can be represented mathematically as follows

$$C_{m_D} = C_{m_D}(a_E) \quad \text{constant} \qquad 0 \leq \omega t \leq \gamma_1 \tag{60a}$$

$$= C_{m_D}(0) + a \qquad \gamma_1 \leq \omega t \leq \gamma_2 \tag{60b}$$

$$= C_{m_D}(0) - ba \qquad \gamma_2 \leq \omega t \leq \gamma_3 \tag{60c}$$

$$= C_{m_D}(a_E) = \text{constant} \qquad \gamma_3 \leq \omega t \leq \pi \tag{60d}$$

in which

$$b = \frac{C_{m_D}(a_E) - C_{m_D}(0)}{a_E} \tag{61}$$

Equations (3), (6), (60), and (61) are combined with Eq (31) to yield the following results for the effective damping of the V-well local damping.

19

$$C_{m_{D_{eff}}}(a_o) = C_{m_D}(a_E) + b\left(\frac{2\theta_1}{\pi}\right)\left(\frac{a_E}{\theta_1}\right)\left[\left(\frac{\gamma_1}{2} - \frac{\sin^2\gamma_1}{4}\right) - \left(\frac{\gamma_3}{2} - \frac{\sin^2\gamma_3}{4}\right)\right]$$

$$+ \frac{a_o}{\theta_1}\left[2\left(\frac{\gamma_2}{2} - \frac{\sin^2\gamma_2}{4}\right) - \left(\gamma_3 - \frac{\sin^2\gamma_3}{4}\right)\right. \tag{62}$$

$$\left. - \left(\frac{\gamma_1}{2} - \frac{\sin^2\gamma_1}{4}\right)\right] + \frac{1}{3}\left[2\sin^3\gamma_2 - \sin^3\gamma_1 - \sin^3\gamma_3\right]\Big\}$$

The final result for the square well is:

$$C_{m_{D_{eff}}}(a_o) = C_{m_D}(a_E) + \frac{2}{\pi}\left[C_{m_D}(a_E) - C_{m_D}(0)\right]\left[\left(\frac{\gamma_1}{2} - \frac{\sin^2\gamma_1}{4}\right) - \left(\frac{\gamma_3}{2} - \frac{\sin^2\gamma_3}{4}\right)\right] \tag{63}$$

In a like manner, other variations of the local damping composed of straight-line (linear) segments can be handled. However, the above results are sufficient to represent large gradients or discontinuities in the local damping near zero angle of attack and predict the balance output under such conditions. For example, Fig. 8b illustrates the rather large effect of oscillation amplitude on the effective damping for an assumed V-well representation of the local damping.

SECTION III
RESULTS AND DISCUSSION

The polynomial curve fit analysis described in Section II has been applied to experimental nonlinear pitch-damping data from the VKF forced-oscillation balance. These data and the acquisition of these data are described in Refs 3 and 4. Table I lists the configurations and associated test conditions that were considered in the present report. The configurations were 60- and 70-deg half angle, blunted, cones with various afterbody arrangements (Fig. 9).

Preliminary investigation revealed that the sixth-order polynomial representation gave better results for the fitted effective damping and computed local damping than either the fourth- or eighth-order polynomials. All the results presented herein are from a sixth-order polynomial curve fit unless stated otherwise. The polynomial analysis gave reasonable results for the majority of the test conditions considered for these configurations.

A certain amount of discretion is necessary when applying this technique and evaluating results. A good polynomial curve fit to the experimental effective damping data does not guarantee that the computed local damping will be realistic. That is, for all practical purposes, the method does not yield a unique solution for the local damping. A slightly different fit to the experimental effective damping may change the computed local damping considerably. The requirement was imposed that the computed local damping must exhibit realistic behavior before the results can be considered satisfactory.

20

TABLE I
VIKING PITCH-DAMPING TEST CONDITIONS*

Configuration	M_∞	$Re_d \times 10^{-6}$	Figure Number
610N	0.70	0.570	10a
↓	1.00	0.440	10b
	1.30	0 390	10c
	1.50	0 580	10d
721	0 70	0.873	11a
	0.80	0.790	11b
	0.90	0.732	11c
	1.00	0.689	11d
	1.10	0.655	11e
	1.20	0.624	11f
	1.40	0.594	11g
	1.55	0 581	11h
	1.60	0 579	11i
	1.90	0.578	11j
	2.30	0 624	11k
	2 65	1 299	11ℓ
↓	3.00	0.730	11m
720	0.70	0 876	12a
	0.80	0.791	12b
	0 90	0.729	12c
	1.00	0 686	12d
	1.10	0 648	12e
	1 20	0 625	12f
	1.40	0 596	12g
	1.53	0 582	12h
	1.90	0 587	12i
	2.30	0 616	12j
↓	3.00	0 732	12k

*From Refs 3 and 4

5. 442 (Typ)
ℓ = 2.679
x_{cg} = 1.887
60 deg (Typ)
1. 450R (Typ)
Pivot Axis
2. 219
10. 000 Diam (Typ)
3. 830 (Typ)

Configuration 610N = 601

x_{cg} = 3.317
ℓ = 2.650 (Typ)
70 deg (Typ)
3. 875R (Typ)
8. 450
Pivot Axis
3. 500
4. 380
15. 500 Diam (Typ)
5. 550
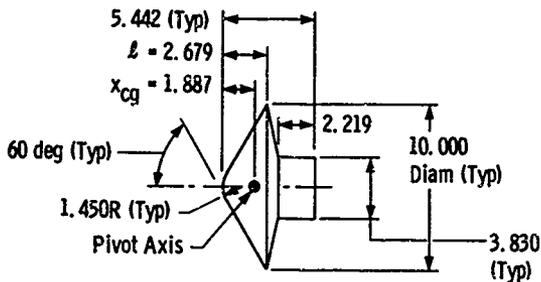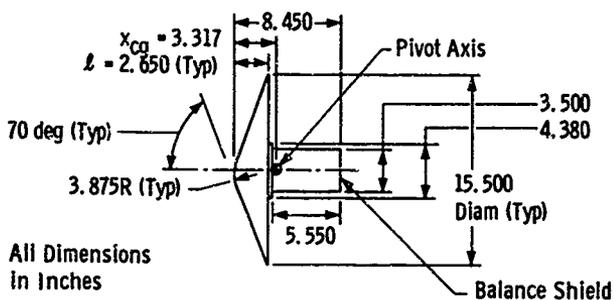
All Dimensions in Inches

Balance Shield

Configuration 720

5. 170
x_{cg} = 3.317
70 deg (Typ)
3. 875R (Typ)
Pivot Axis
6. 135
2. 870
15. 500 Diam (Typ)
11. 388
ℓ = 2.650 (Typ)
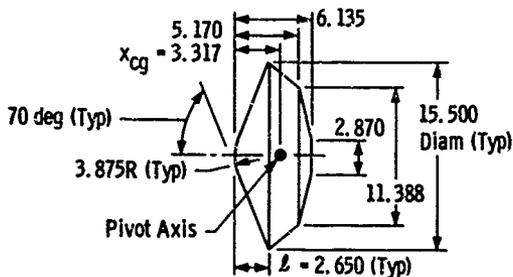
Configuration 721
Fig. 9 Model Geometry

22

The results are presented in Fig. 10 (Configuration 610N), Fig. 11 (Configuration 721), and Fig. 12 (Configuration 720) as a function of angle of attack. Shown are the spread in the experimental data (vertical lines), the sixth-order fit to the experimental data of equivalent damping (dashed line), and the computed local value. For all cases the damping is stabilizing at higher angles and varies from mildly stabilizing to violently destabilizing at zero angle of attack.

Figure 13 presents a summary of the damping coefficient at zero angle of attack versus Mach number. The basic character of the curve is the same for each configuration, i.e., near-neutral stability at a Mach number of 0.7, becoming significantly unstable in the Mach number range from 1 0 to 2.2, and stable at higher Mach numbers

Satisfactory results for polynomial representation could not be obtained for Configurations 720 and 721 at M_∞ = 1.40 to 1.90 The balance output for these conditions (Figs. 11g, h, i, j, and 12g, h, i) reveals that the experimental effective damping has an extremely strong (almost discontinuous) variation between a of zero and 1 deg. Also shown in these figures are the results of the effective damping computed from an assumed V-well variation of the local damping. Other variations of the V-well and square well representations, as well as polynomial curves, were also investigated, but the computed effective damping did not change substantially from that shown in these figures This computed effective damping and the experimental effective damping differ considerably at a = 1 deg, but compare favorably at a = 0 and 2 deg

For M_∞ = 1.20 to 2.0, it is possible that the highly nonlinear behavior observed in the experimental effective damping could be attributed to a destabilizing hysteresis effect in the static pitching moment and that these effects are greatest at a_o = 0 (Eq (29)). The mathematical nature of the curve suggests this possibility, but there is no relevant aerodynamic theory upon which to base this speculation Free-oscillation data (for various amplitudes and frequencies) will shed some light on this.

SECTION IV
SUMMARY AND CONCLUSIONS

A procedure to extract the local damping from the experimental effective damping output of a forced-oscillation balance has been derived because the local instantaneous pitch damping is required for motion simulation of certain preliminary Mars unmanned reentry (Viking) configurations. The VKF forced-oscillation pitch-damping balance system has been briefly reviewed and a relationship has been established between the effective damping output of the balance and the local aerodynamic damping. This relationship is an integral equation which was solved to yield a practical connection between the local and effective damping. This connection involves a high-order polynomial (up to eighth order in a and θ_1) representation of the damping coefficients. Practical use of this technique requires a polynomial curve fit to the experimental effective damping which results in coefficients for the polynomial representation of the local damping. This procedure has been applied to experimental data obtained by the VKF forced-oscillation balance for preliminary Viking configurations.

The following characteristics of the procedure and conclusions concerning its practical usage are noteworthy:

1. Initial attempts to obtain a practical solution for the integral equation (Eq. (31)) utilized a Fourier series representation of the local damping and also a discrete variable approach. Both of these methods were unsatisfactory and were abandoned in favor of a polynomial representation which proved successful.

2. Discretion is necessary when applying the polynomial curve-fitting technique and interpreting the results. A good polynomial curve-fit to the experimental effective data does not automatically yield reasonable results for the computed local damping. The computed local damping also has to exhibit realistic behavior before the overall results can be considered satisfactory.

3. The sixth-order polynomial representation gave better overall results for the fitted effective damping and the computed local damping than either the fourth- or eighth-order polynomials.

4. The present polynomial technique may be applied to free-oscillation damping data acquired by oscillating about $a = 0$, if a_0 is set equal to zero in Eq (39).

5. The polynomial method may also be applied to free-oscillation data obtained by small oscillation about a nonzero a_0. In this case, the free-oscillation damping must be determined for the same value of θ_1 from the oscillation envelopes obtained by testing at different values of a_0.

6. If the static moment is a multivalued function of a for an oscillation cycle (hysteresis), this will create additional damping (or undamping) which will add to any conventional aerodynamic damping already present The balance output will contain the sum of both the hysteresis damping and conventional damping. Forced- or free-oscillation test data for different amplitudes and frequencies will aid in interpreting this phenomenon.

7. The apparent damping effects of a multivalued static aerodynamic pitching moment are not included in the integral equation (Eq. (31)) relating local and effective aerodynamic damping. This also applies to the polynomial solution of the integral equation (Eqs. (34) and (39)).

8. The polynomial method gave reasonable results for the Mars unmanned reentry configurations at the subsonic, transonic, and supersonic Mach numbers above $M_\infty = 2.00$. However, reasonable results could not be obtained for Configurations 720 and 721 at Mach numbers from 1.40 to 1.90.

a. $M_\infty = 0.70$

b. $M_\infty = 1.00$
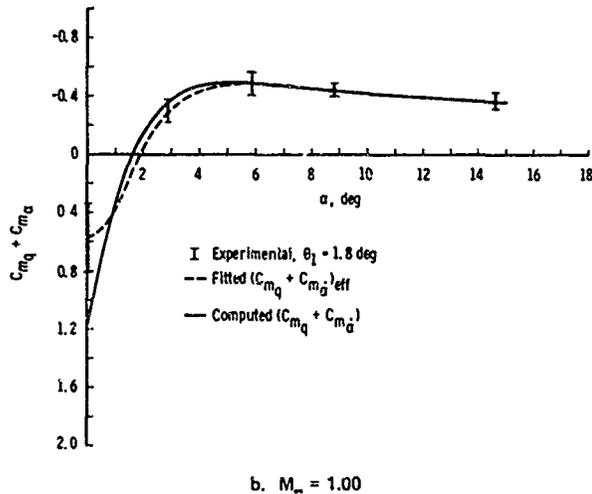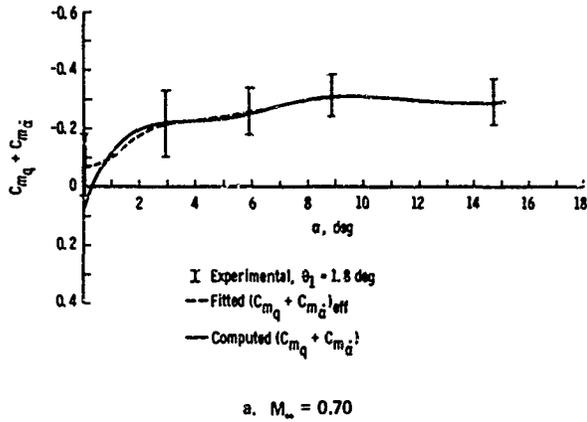
Fig. 10 Local and Effective Pitch-Damping Coefficients versus Angle of Attack for Configuration 610N
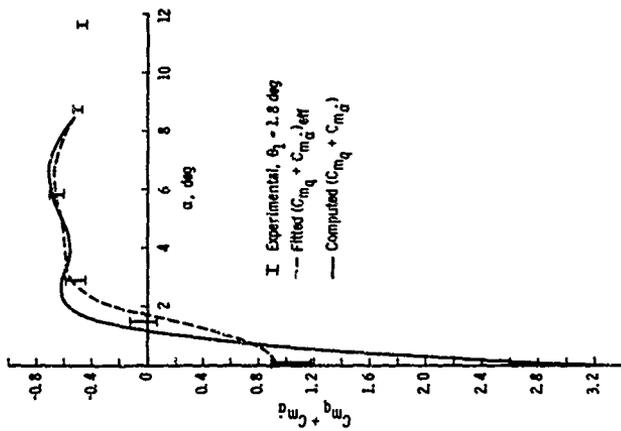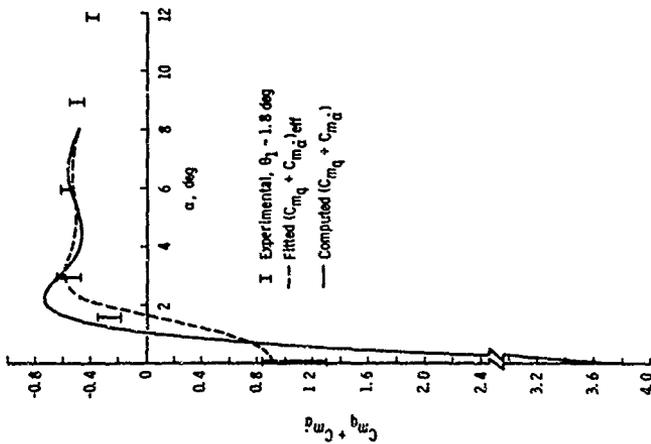
c. $M_\infty = 1.30$

d. $M_\infty = 1.50$

Fig. 10 Concluded
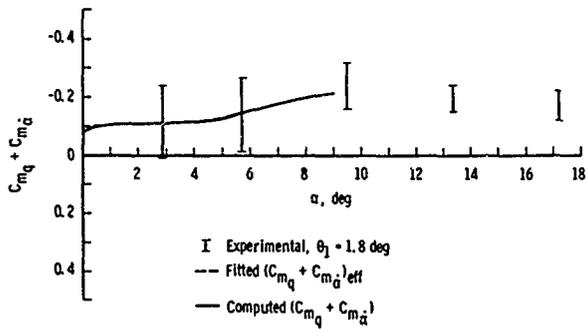
a. $M_\infty = 0.70$
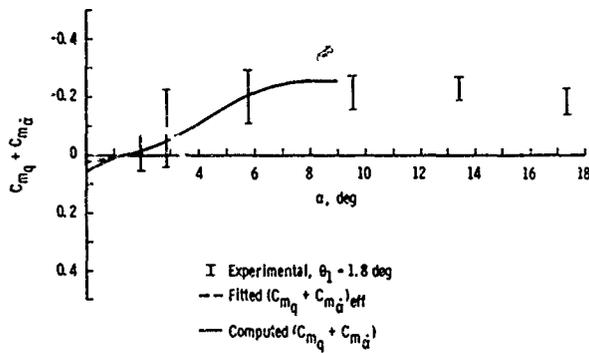
b. $M_\infty = 0.80$

Fig. 11 Local and Effective Pitch-Damping Coefficients versus Angle of Attack for Configuration 721
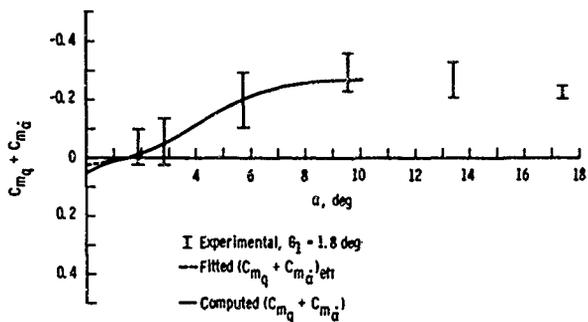
c. $M_\infty = 0.90$
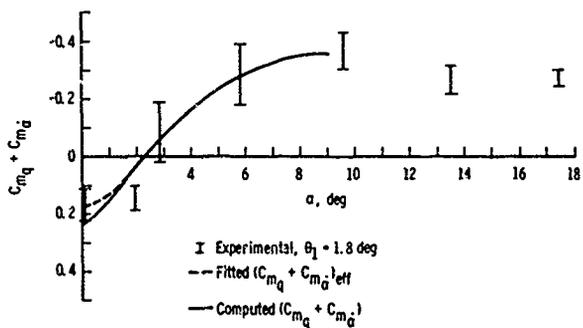
d. $M_\infty = 1.00$
Fig. 11 Continued

28

e. $M_\infty = 1.10$

f. $M_\infty = 1.20$

Fig. 11 Continued

29

g. $M_\infty = 1.40$

h. $M_\infty = 1.55$

Fig. 11 Continued

30
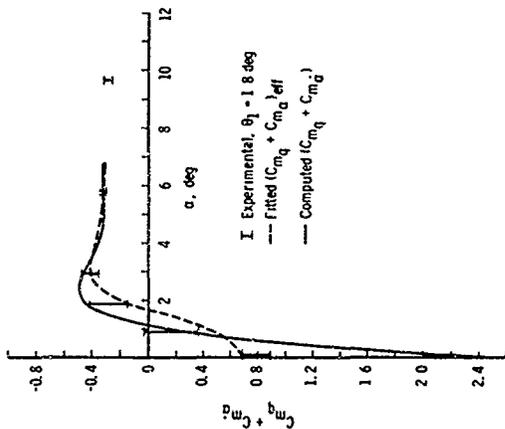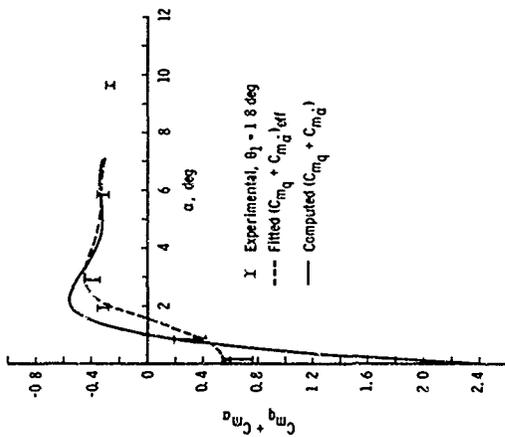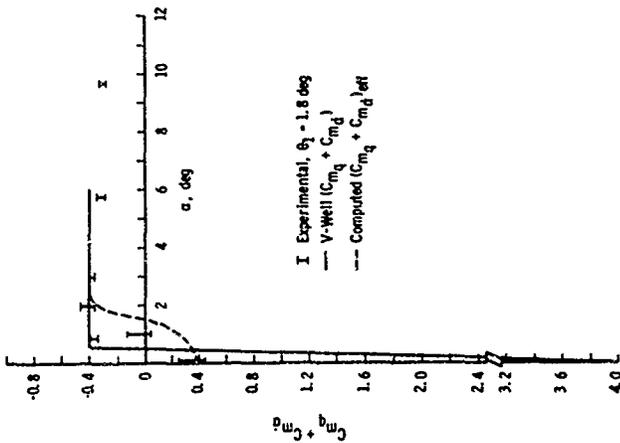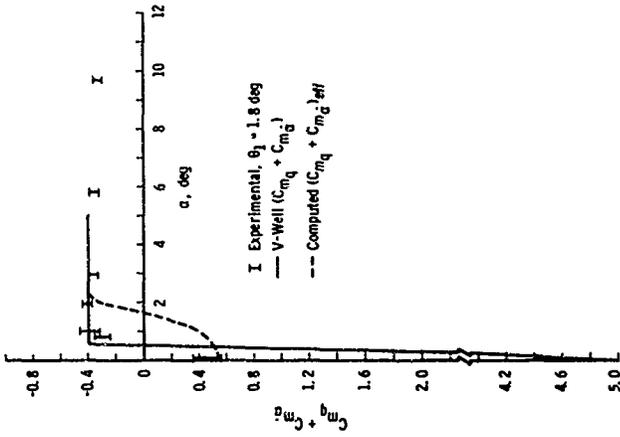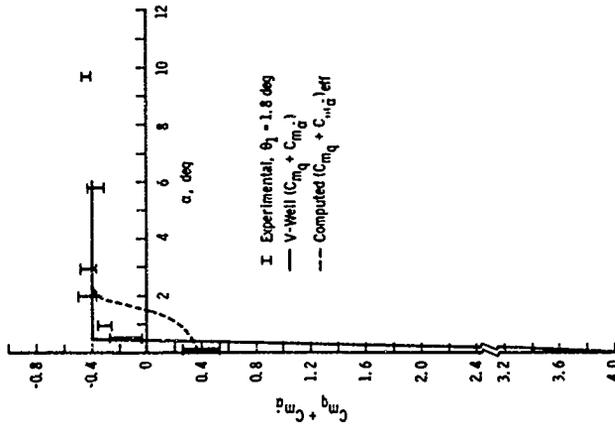
j. $M_\infty = 1.90$
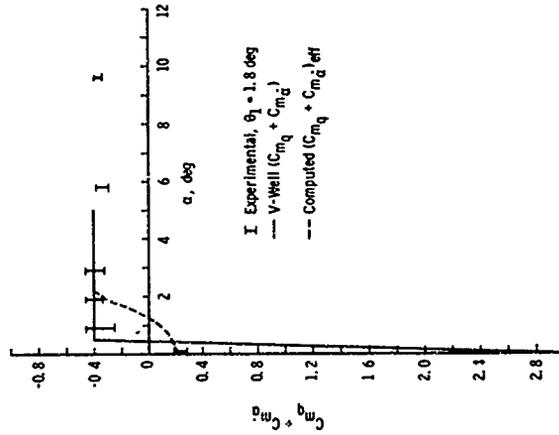
i. $M_\infty = 1.60$

Fig. 11 Continued

31
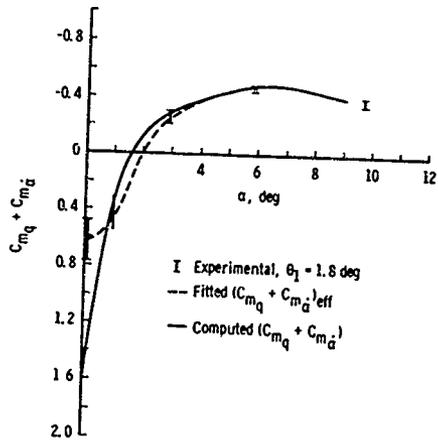
k. $M_\infty = 2.30$
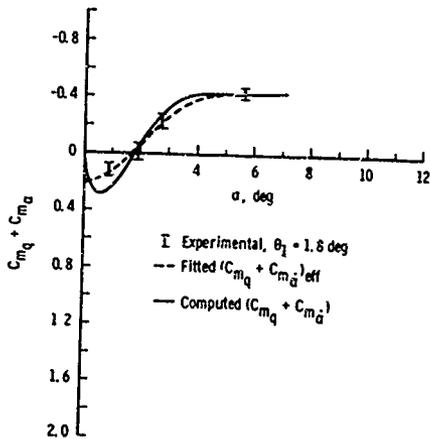
l. $M_\infty = 2.65$
Fig. 11 Continued
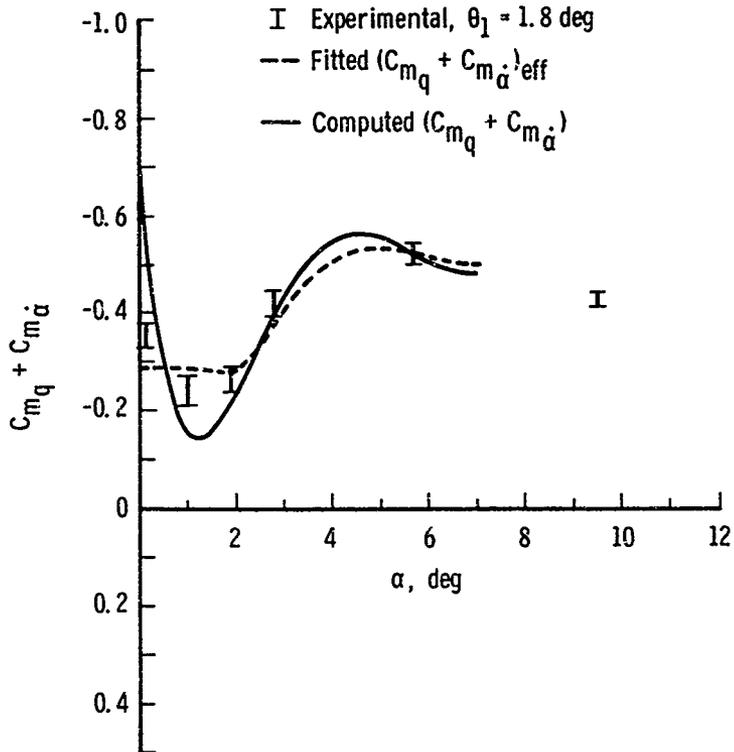
m. $M_\infty = 3.00$
Fig. 11 Concluded
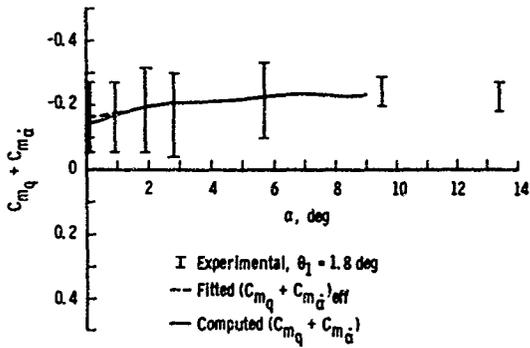
a. $M_\infty = 0.70$
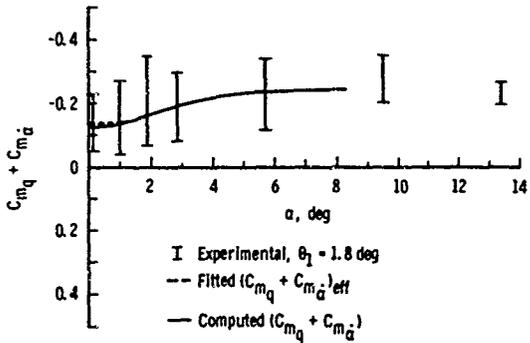
b. $M_\infty = 0.80$

Fig. 12 Local and Effective Pitch-Damping Coefficients versus Angle of Attack
for Configuration 720
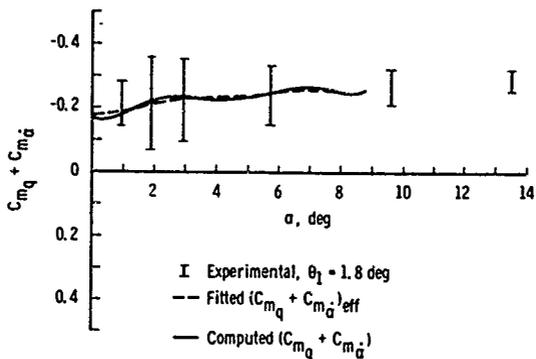
c. $M_\infty = 0.90$
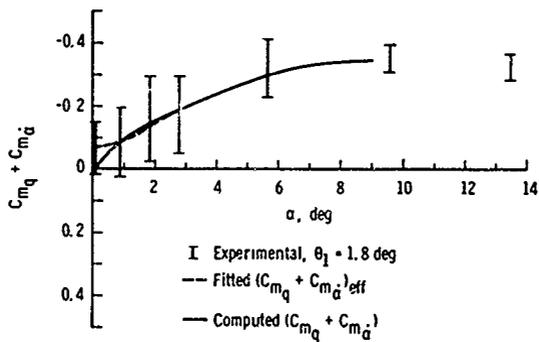
d. $M_\infty = 1.00$
Fig. 12 Continued
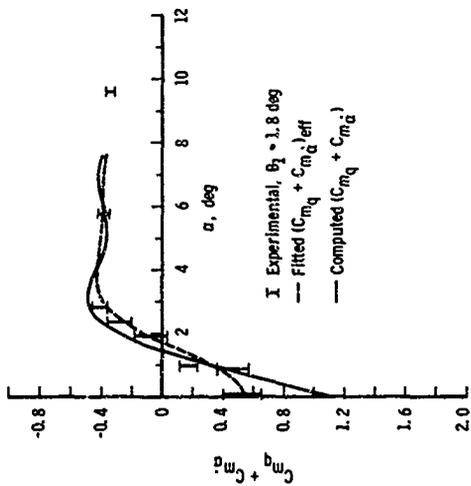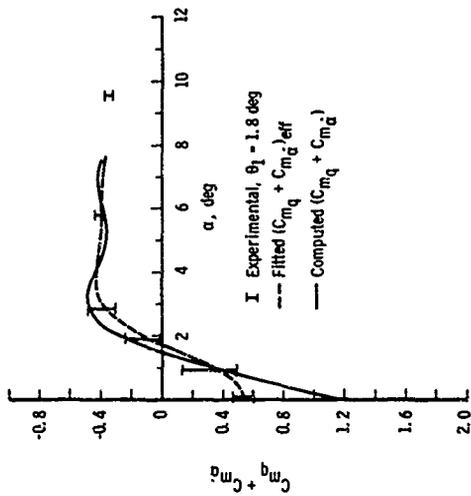
e. $M_\infty = 1.10$

f. $M_\infty = 1.20$

Fig. 12 Continued

36
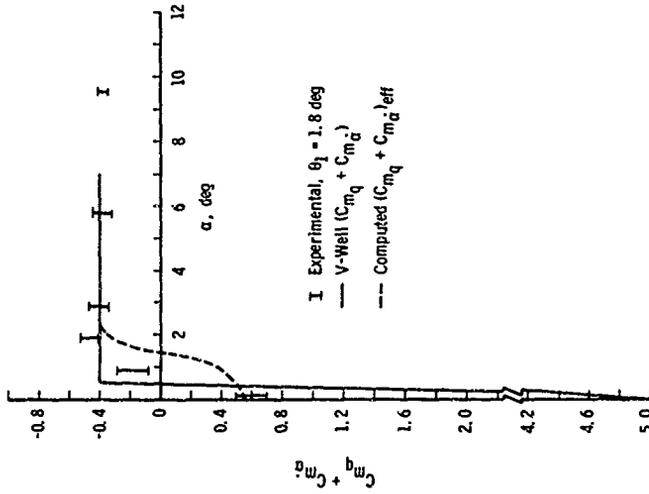
h. $M_\infty = 1.53$
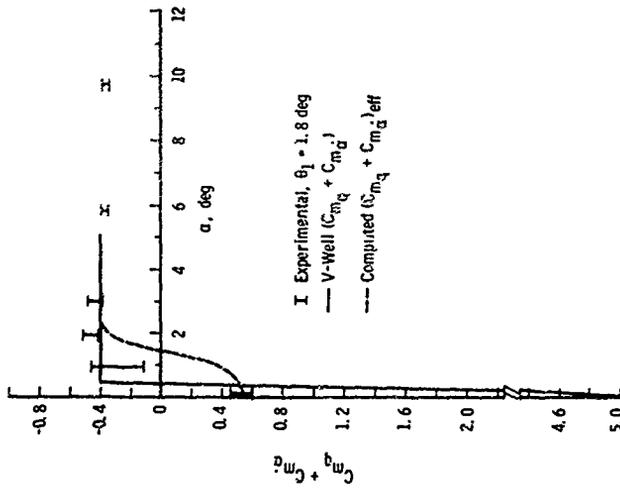
g. $M_\infty = 1.40$

Fig. 12 Continued
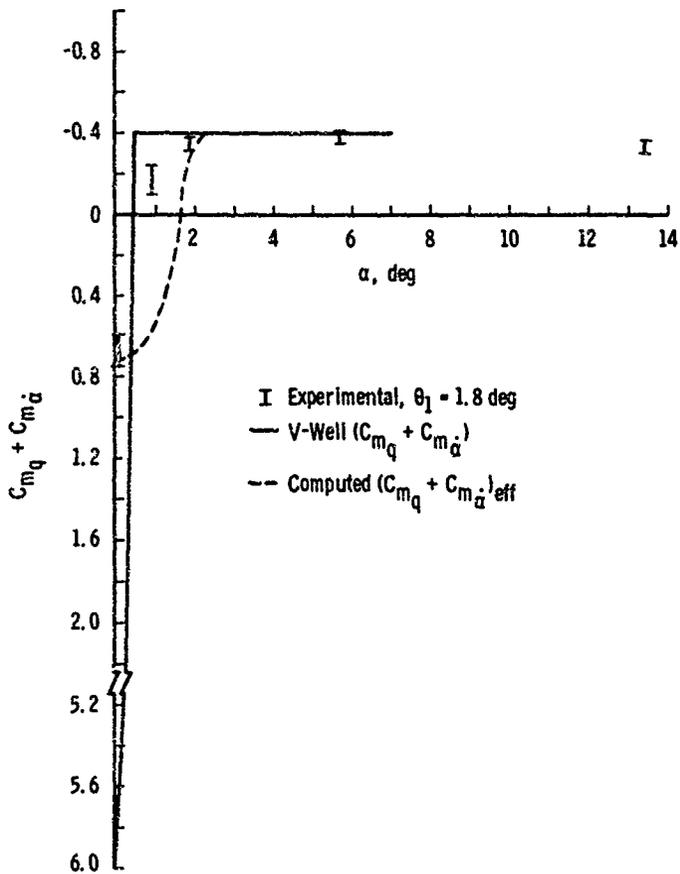
i. $M_\infty = 1.90$
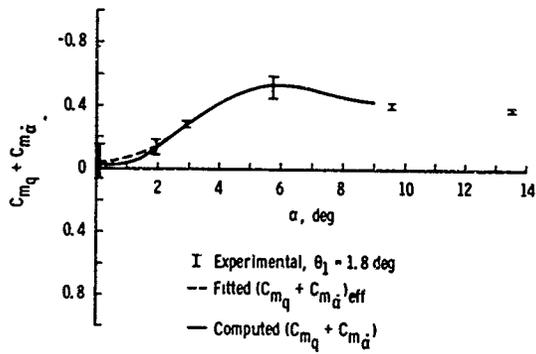
j. $M_\infty = 2.30$
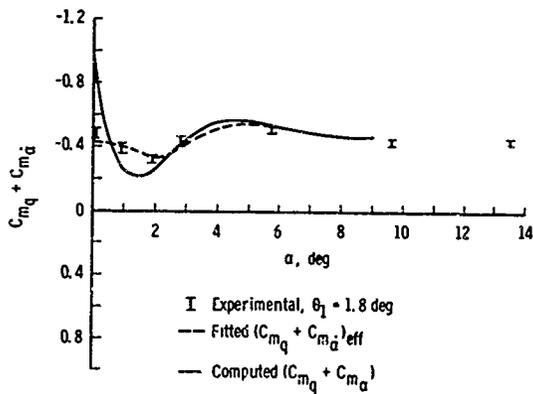
k. $M_\infty = 3.00$
Fig. 12 Concluded
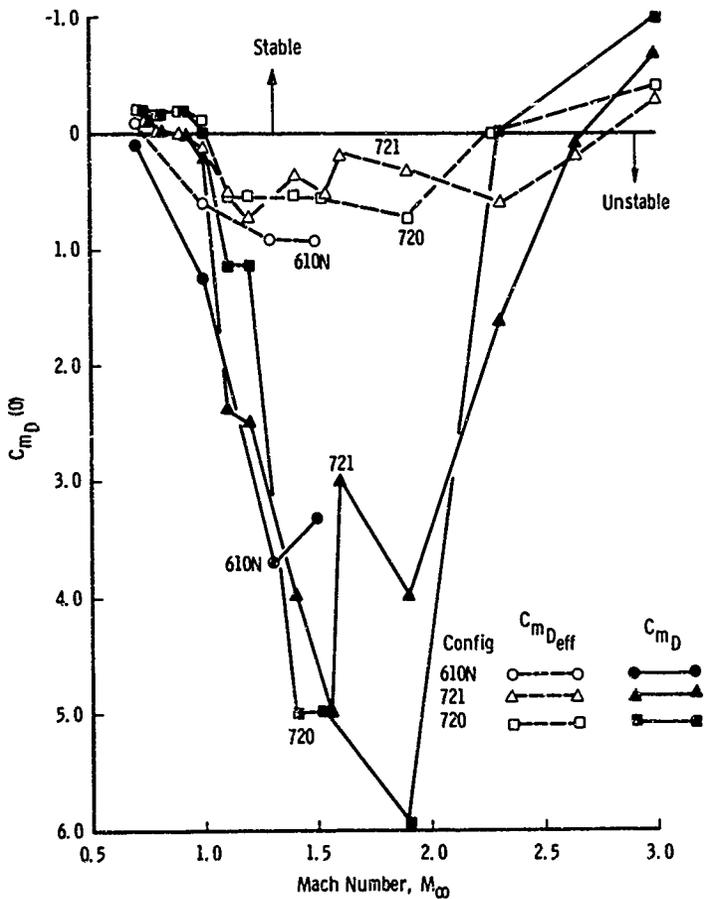
Fig. 13 Summary of Results for Damping at Zero Angle of Attack

REFERENCES

1. Schueler, C. J., Ward, L. K., Jr, and Hodapp, A. E., Jr. "Techniques for Measurement of Dynamic Stability Derivatives in Ground Test Facilities." AGARDograph 121 (AD669227), October 1967.

2. Ward, L. K., Jr., Welsh, C. J., and Hance, Q. P. "A Forced-Oscillation Balance System for the von Karman Gas Dynamics Facility 40- by 40-Inch Supersonic Tunnel." AEDC-TN-61-63 (AD257380), May 1961.

3. Uselton, B. L., Shadow, T. O, and Mansfield, A. C. "Damping-in-Pitch Derivat ·· of 120 and 140-Deg Blunted Cones at Mach Numbers 0 6 through 3 ·' AEDC-TR-70-49 (AD868237L), April 1970

4. Steinberg, S. "Experimental Pitch Damping Derivatives for Candidate Viking Entry Configurations at Mach Numbers from 0.6 through 3.0." Martin Marietta Corporation, Denver Division, TR-3709005, June 1970

5. Kryloff, N. and Bogoliuboff, N "Introduction to Non-L 'ar Mechanics" Translated by Solomon Lefshetz. Princeton University Press, 1947.

6. Redd, B., Olsen, D. M., and Barton, R. L. "Relationship between the Aerodynamic Damping Derivatives Measured as a Function of Instantaneous Angular Displacement and the Aerodynamic Derivatives Measured as a Function of Oscillation Amplitude" NASA-TN-D-2855, June 1965 (See also comments on this paper (No. 11) in Vol. I of the Transactions of the Second Technical Workshop on Dynamic Stability Testing, April 20-22, 1965)

7. Jaffe, P. "A Generalized Approach for Dynamic Stability Analysis" Transactions of the Second Technical Workshop on Dynamic Stability Testing, April 20-22, 1965, Vol. I, Paper No. 13.

8. Morse, P M. and Feshbach, H Methods of Theoretical Physics Vol I, Chapter 8, McGraw-Hill Book Co., New York, 1953

9. Lovitt, W. V. Linear Integral Equations McGraw-Hill Book Co, New York, 1924, reprinted by Dover Publishing Company, 1950

10 Judd, M. "Methods for the Wind-Tunnel Measurement of Unsteady Nonlinear Aerodynamic Forces." AIAA Journal, Vol. 9, No. 7, July 1971, pp. 1302-1307